ADVANCES IN AGRICULTURAL AND FOOD RESEARCH JOURNAL

Original Research Article

Computational Studies on the Effects of a Central Shaft and a Guiding Wall on the Savonius Hydrokinetic Turbine Performances

Komsan Tantichukiad[1,*], Azmi Yahya[2], Anas Mohd Mustafah[2], Hazreen Haizi Harith[2], Azmin Shakrine Mohd Rafie[3], Ahmad Suhaizi Mat Su[4]

[1]Department of Mechanical and Manufacturing Engineering, Universiti Putra Malaysia, 43400 Serdang, Selangor D.E., Malaysia, mi_kom@hotmail.com

[2]Department of Biological and Agricultural Engineering, Universiti Putra Malaysia, 43400 Serdang, Selangor D.E., Malaysia, azmiy@upm.edu.my

[3]Department of Aerospace Engineering, Universiti Putra Malaysia, 43400 Serdang, Selangor D.E., Malaysia, shakrine@upm.edu.my

[4]Faculty of Agriculture, Universiti Putra Malaysia, 43400 Serdang, Selangor D.E., Malaysia, asuhaizi@upm.edu.my

*Corresponding author: Komsan Tantichukiad, Department of Mechanical and Manufacturing Engineering, Universiti Putra Malaysia, 43400 Serdang, Selangor D.E., Malaysia; mi_kom@hotmail.com

Abstract: Most wetland rice production schemes have good networks of irrigation and drainage canals built for the benefit of the farmers to perform farming activities. The canals have ample volume of running water all year round and could be harnessed for hydropower. The Savonius hydrokinetic turbine has been generally used to generate electrical energy as the means of renewable source over fossil fuels. Numerous parameters have been studied to enhance the performance of the turbine. However, the turbine power performance is still low as compared to other types even though it is known to have excellent torque characteristics. Therefore, the objectives of this study are to evaluate the effects of a central shaft and a guiding wall on the performances of the Savonius hydrokinetic turbines by using two-dimensional computational simulations. ANSYS Fluent software with the standard k-ε turbulence model and dynamic mesh motion techniques were used to get the optimum central shaft and guiding wall configurations. The central shaft was studied in three cases; (I) with a full shaft, (II) with a shaft and space, and (III) without shaft between two end plates. Moreover, the turbine performances were also evaluated with and without the presence of a guiding wall. The turbine performances were computed. Simulation results e.g. velocity, pressure contours and flow structures across a SHKT model were analysed and discussed.

Keywords: Savonius hydrokinetic turbine; computational fluid dynamics; turbine central shaft; turbine guiding wall; flow structures

Received: 8th June 2020

Received in revised form: 10th December 2020

Accepted: 30th January 2021

Available Online: 15th February 2021

Citation: Tantichukiad, K., Yahya, A., Mohd Mustafah, A., *et al.* (2021). Computational studies on the effects of a central shaft and a guiding wall on the Savonius hydrokinetic turbine performances. *Adv Agri Food Res J 2021*; In-Press: a0000253. https://doi.org/10.36877/aafrj.a0000253

1. Introduction

For more than half a century, developing and developed countries have been concerned about global warming situations caused by greenhouse gases (GHGs) especially carbon dioxide (CO_2). These countries have been trying to reduce fossil fuels combustion and GHGs emissions by using renewable energy sources. Hydropower or hydrokinetic energy is a type of renewable energy captured from the kinetic energy of water flow. It is a promising solution to solve these issues. In order to produce clean and green energy, mechanical devices commonly known as turbines are utilised to transform hydrokinetic energy into electricity.

The majority of granary areas in Malaysia have good meshes of irrigation and drainage canals that are suitable for agricultural activities. This infrastructure is not only good for planting activities, but it also has the potential to be used to generate electricity. All year-round, these canals have sufficient water in terms of volume and velocity that can generate electricity by setting up a turbine across the flow. There are various types of turbines based on their characteristics such as sizes, operational characteristics and direction of the turbine axis. Therefore, turbine selection needs to be optimised by considering several factors including sizes of irrigation canal, flow conditions and turbine performances. A vertical axis Savonius hydrokinetic turbine (SHKT) was chosen in this study because it has unique advantages such as the excellent starting torque and simplicity of designs compared to other types of turbines. Moreover, the structure is simple and easy to fabricate with a low construction and maintenance cost. It is able to operate at any flow direction (Mahmoud *et al*., 2012, Akwa *et al*., 2012).

In the last couple of decades, many parameters of Savonius either wind or hydro turbines have been studied either experimentally or computationally. Researchers found that the performances were depended on the turbine operational conditions, geometric parameters, and fluid flow conditions (Akwa *et al*., 2012). In this study, in order to design an optimum and simple SHKT, the optimum geometric parameters such as shape of bucket profile, bucket number and end plates were identified importantly. Furthermore, many previous studies mentioned that a conventional Savonius turbine is poor in operational performances especially at a high-speed ratio, and having a low hydrodynamic efficiency. However, it provides a good starting torque. Therefore, parameters that affect the torque and power performances need to be considered including the effects of the turbine central shaft and a guiding wall.

A central shaft related with the variety of overlap ratio (β) influences the performances of a conventional Savonius turbine. Theoretically, the overlap ratio is defined as a ratio of the space or overlap length (e) between two buckets, to the chord length of a turbine bucket or the bucket diameter (D_b) if that bucket is semi-circular (Mahmoud *et al*., 2012). It can be expressed in Equation (1) (Akwa *et al*. 2012, Damak *et al*. 2013, Jahangir Alam *et al*. 2009). Whereas the overlap ratio of a Savonius turbine with a central shaft having

a diameter (d) can be determined by Equation (2) (Mahmoud *et al*. 2012, Damak *et al*. 2013, Jahangir Alam *et al*. 2009). It means that an overlap ratio equals to zero ($\beta = 0$) in the case of a turbine having a full central shaft ($d = e$) or no space between buckets ($e = 0$). Whereas, it equals to e/D_b in case of a turbine has no shaft.

$$\beta = \frac{e}{D_b} \tag{1}$$

$$\beta = \frac{e - d}{D_b} \tag{2}$$

A large number of studies that investigated the influence of overlap ratios have been carried out using experimental and computational approaches. It can be summarised that there are two major conflicts on the conclusions of the optimum β as stated in Table 1. Besides that, the results depicts in Figure 1 shows the variation of c_p of Savonius either wind or hydro turbines. The maximum c_p occurred when β is equal to zero and not equal to zero as shown in Figure 1(a) and (b), respectively.

Table 1. Determination of overlap ratio effect.

Researchers	Methodology	Turbine	Range used	Optimum β	Optimum c_p and c_t
Saad *et* ail., 2020	3D Numerical wind	A 45º twisted Savonius rotor	0, 0.1, 0.15, 0.2, 0.3	0	c_p = *0.223*, c_t =*0.38 at* U_∞ = *6 m/s*
M. A. Kamoji *et al*., 2009	Experimental wind	A modified Savonius rotor, without shaft	0, 0.1, 0.16	0	c_p = 0.17 at Re=1.5×10^5
M. A. Kamoji *et al*., 2009	Experimental wind	A 90º twisted helical Savonius rotor	0, 0.1, 0.16	0	c_p = 0.175 at λ = 0.9,Re=1.5×10^5
Mahmoud *et al*., 2012	Experimental wind	Two bladed semi-circular	0, 0.2, 0.25, 0.3, 0.35	0	-
Kianifar & Anbarsooz, 2011	Experimental & Numerical wind	Two bladed Savonius turbine	0, 0.20, 0.24, 0.40, 0.45	0.2	c_p= 0.254 @Re=1.5×10^5
Roy & Saha, 2013a	2D Numerical wind	Two bladed Savonius turbine	0 - 0.30	0.2	c_{ts} = 0.224 at U_∞= 10.44 m/s
Yaakob *et al*., 2010	3D Numerical Hydro	Savonius turbine with double stage	0.1 - 0.6	0.21	τ_{avg}= 0.1362 at U_∞ = 0.169 m/s
Menet *et al*., 2004	2D Numerical wind	Double stepped Savonius with two paddles and end plates	0.1-0.5	0.242	c_t = 0.33 at Re=1.56×10^5
Zhao *et al*., 2009	3D Numerical wind	Two bladed 180º helical Savonius rotors	0.0, 0.2, 0.3, 0.4, 0.5	0.3	c_p = 0.181 at λ = 0.73
Mabrouki *et al*., 2014	Experimental Hydro	Two blades Savonius turbine	0, 0.2, 0.3	0.3	c_p = 0.327 at Re=588,300

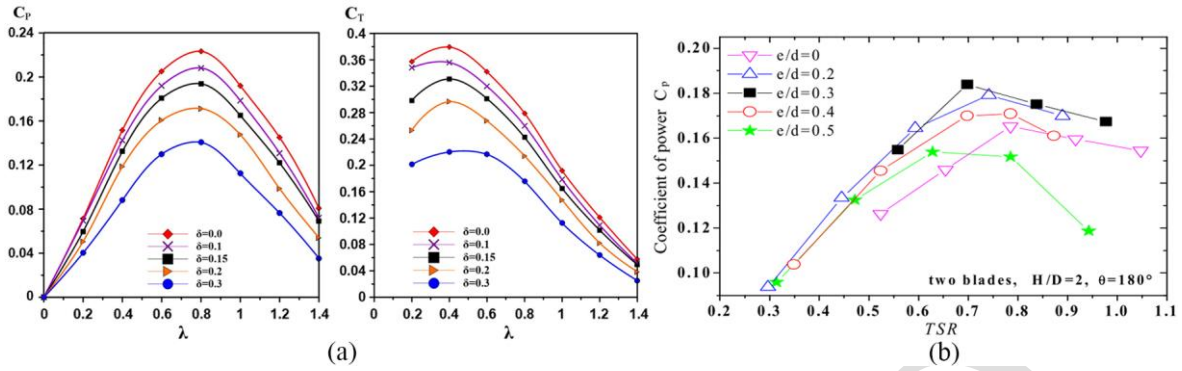

Figure 1. The best performances occurred when **(a)** β is equal to zero (Saad *et al*., 2020) and **(b)** β is not equal to zero (Zhao *et al*., 2009).

In order to improve torque characteristics, several studies on the effects of the guiding wall called in this paper, or also known as deflector plate, obstacle shielding or convergent nozzle have been carried out using either wind or hydro turbine. The guiding wall parameters were studied experimentally or computationally such as designed shape (Kerikous *et al*., 2019, and Altan and Atilgan 2008), the optimal position (Kailash *et al*., 2012), or the influence of the location (Golecha *et al*., 2011)., However, there is no information with the design that a guiding wall is fully covered from a returning bucket to one side of the wall domain. Meaning that previous designs of the guiding walls have been focusing on keeping the same frontal area between with and without the presence of the guiding walls. Table 2 summarises the experimental and numerical results of the previous studies on the effects of one, or two guiding walls.

Table 2. Summary of studies on effects of the guiding wall.

Researchers	Types of guiding plate	Methodology	Turbine	Coefficient of performance
Mohamed *et al*., 2010	One straight plate	Numerical	Savonius wind turbine	c_p increases 27.3% for two blades and 27.5% for three blades
Golecha *et al*., 2011	One straight plate	Experimental	Savonius hydro turbine	c_p increases 50% for modified Savonius turbine
El-Askary *et al*., 2015	Curved plates	Numerical	Savonius wind turbine with complex geometry	c_p increases 160% for modified Savonius turbine
Kailash *et al*., 2012	Two deflector plates	Experimental	Savonius hydro turbine	c_p increases 150% for modified Savonius turbine

In order to enhance the performances of a SHKT model, the present study aims to evaluate the effects of a turbine central shaft design and a guiding wall on the performances of a SHKT model by using 2D CFD simulations. ANSYS Fluent software with the standard *k-ε* turbulence model and dynamic mesh motion techniques were used to get the optimum

central shaft design and guiding wall characteristics for the turbine. The turbine central shaft was studied in three cases; (I) with a full shaft, (II) with a shaft and space, and (III) without shaft between two end plates. Moreover, the turbine performances were also evaluated with and without the presence of a guiding wall.

2. Materials and Methods

2.1. Performance parameters

Theoretically, the rate of kinetic energy change of a water stream with velocity U_∞ flowing through an area A with mass flow rate $\rho A U_\infty$ can be represented in terms of the hydrokinetic power (P_{Hydro}; watts) as written in Equation (3). P_{Hydro} is converted into shaft power (P_s) or mechanical power (P_m) by turbines. Two dimensionless parameters have been identified to determine the turbine performances. The first one is the power coefficient (c_p) which is a ratio of P_m to P_{Hydro} as derived from Equation (4) and the other one expressed in Equation (5) is the torque coefficient (c_τ). Further, the relationship between c_p and c_τ is as stated in Equation (6) where λ is the tip speed ratio (TSR) which is a ratio between the tangential velocity of the turbine (v) and upstream flow velocity (U_∞).

$$P_{Hydro} = \frac{1}{2}\rho U_\infty^3 A = \rho H_s R_s U_\infty^3, \text{ and } P_m = \tau\omega \tag{3}$$

$$c_p = \frac{P_m}{P_{Hydro}} = \frac{\tau\omega}{\rho H_s R_s U_\infty^3} \tag{4}$$

$$c_\tau = \frac{\tau}{\frac{1}{2}\rho A R_s U_\infty^2} \tag{5}$$

$$c_p = \lambda c_\tau \tag{6}$$

2.2. Computational methodology

The detailed designs of a SHKT model and the modified ones with variations of a central shaft configuration and a guiding wall as well as the computational approaches are described in this subsequence.

2.2.1. Design of a SHKT model

To get an optimum designed shape of a SHKT model, several parameters need to be considered. It was found that the optimum bladed number was two (Zhao *et al*., 2009, Parag K. Talukdar *et al*., 2018, Mahmoud *et al*., 2012). The semi-circular shape of buckets is better than the elliptic (Parag K. Talukdar *et al*., 2018, Kacprzak, *et al*., 2013). A conventional Savonius turbine with a circular shape (Jeon *et al*., 2015), and with upper and lower end plates (Saad *et al*., 2020) performed better performance. Besides that, it was found that the optimum end plate diameter (D_e) was 1.1 times of the rotor diameter (D_r) (Sivasegaram 1978,

Fujisawa 1992, Saad *et al*., 2020). The aforementioned parameters were combined to develop a SHKT model as called a standard SHKT model shown in Figure 2(a) by using Computer Aids Design (CAD) commercial software. A standard SHKT model was designed with a height of 0.1 m. and made from stainless steel (ρ_{ss}=7,800 kg/m^3). A schematic diagram and the detailed specifications of a standard SHKT model are presented in Figure 2(b) and Table 3.

To investigate the influences of a central shaft, then the modifications of a standard SHKT model were carried out. A central shaft was designed and varied into three cases; (I) with a full shaft, (II) with a shaft and space, and (III) without shaft as shown in Figure 3(a). Based on the geometry of a standard SHKT model, the overlap length (e) between two buckets of 0.006 m. depicted in Figure 2(b) was fixed, while the turbine shaft diameter (d) was varied. So that, the overlap ratios (β) of case I, case II and case III were 0, 0.0009 and 0.06, respectively.

A standard SHKT model was modified with a guiding wall as shown in Figure 3(b). As presented in Figure 3(b), one end of a guiding wall is located along the centre line and far away from the turbine centre (S_G) while another end is mounted with a side of domain walls. The incline angle (α) is 45^o. Guiding wall configurations are described in Table 3.

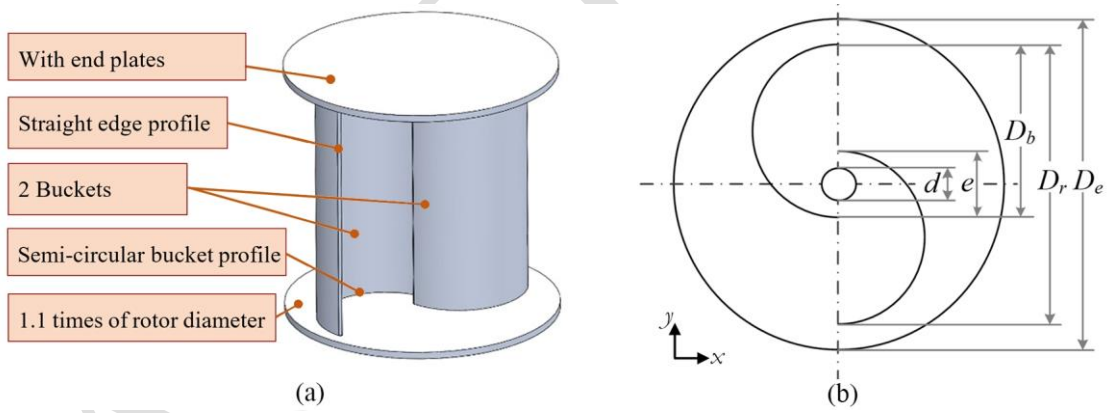

Figure 2. **(a)** A standard SHKT model and **(b)** Schematic diagram of a standard SHKT model.

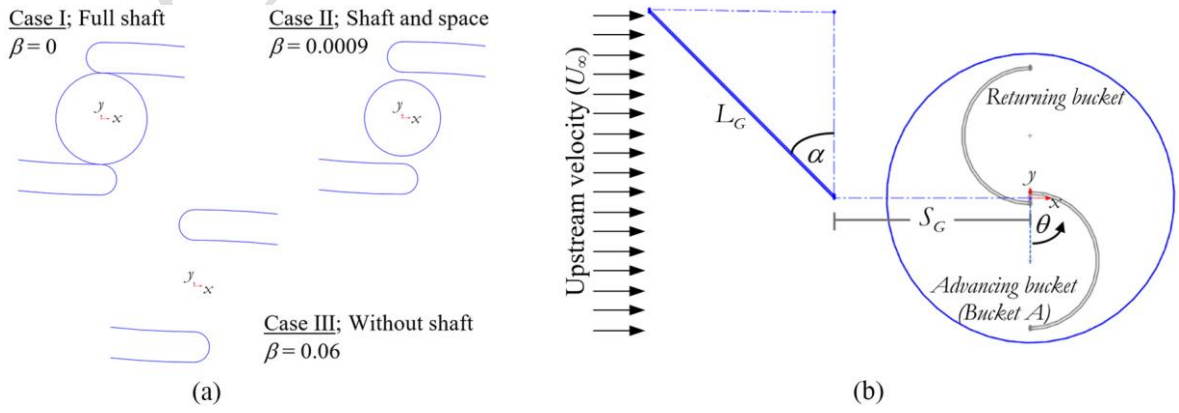

Figure 3. **(a)** Design of modified turbines with effects of a centre shaft and **(b)** design of a guiding wall configuration.

Table 3. Detail specifications of simulated SHKT design.

Model	Parameters	Value		
A standard SHKT model	Rotor diameter (D_r)		0.2 m	
	Bucket diameter (D_b)		0.100 m	
	End plate diameter (D_e)		0.202 m	
	Bucket thickness (t_s)		0.002 m	
Modified with a central shaft	Shaft diameter (d)	0	0.00591 m	0.006 m
	Spacing (e-d)	0.006 m	0.00009 m	0
Modified with a guiding wall	Length (L_G)		0.424 m	
	Distance from a centre of SHKT (S_G)		0.150 m	
	Incline angle (α)		45^o	

2.2.2. Computational domain and boundary conditions

The computational domain is also important in the CFD simulation. In fact, the domain size is described in terms of a proportion of a rotor diameter (D_r). The dimension of the domain was designed following the published literature such as, Mendoza *et al*. (2020), Saad *et al*. (2020), Yaakob *et al*. (2010), and so on, to confirm negligible effects of domain walls on the SHKT performances. To assure of the negligible domain wall effect, the bigger the domain size, the better the simulated accuracy. However, the oversize domain might take more computational costs such as bigger hard disk spaces and longer simulation time. Kumar *et al*., (2016) and Kumar and Saini (2017) set the domain width of 3.4D and length of 18.75D in their CFD studies and found that the minimum domain width and length did not interfere with flow filed across the turbine.

In the present study, therefore, a two dimensional domain and its boundary conditions were imposed illustrated in Figure 4(a). The domain was a symmetrical rectangular, and a SHKT model was located at the centre of the domain which separated the domain into front-back regions and upper-lower regions equally. The domain width and length were designed as three times ($3D_r$) and six times ($6D_r$) of a SHKT diameter, respectively.

The computational technique utilised in this study was a dynamic mesh motion technique where its domain was divided into two main regions. The first one is called a rotating region or an inner domain that contains the areas around a SHKT and another is called a stationary region or an outer domain. Both regions were separated by the interface line to ensure the continuity of the flow field (Kumar & Saini, 2017). In addition, symmetrical boundary conditions were imposed for all lateral walls. The uniform and constant upstream velocity (U_∞) enters perpendicularly at the inlet boundary. U_∞ was varied into four values including 0.3 m/s, 0.5 m/s, 0.8 m/s and 1.1 m/s. The total pressure was imposed at the outlet

boundary. A 5% turbulent intensity (I_t) was determined for all simulations. Finally, the no-slip boundary condition was defined at all surface areas of a SHKT model and lateral walls.

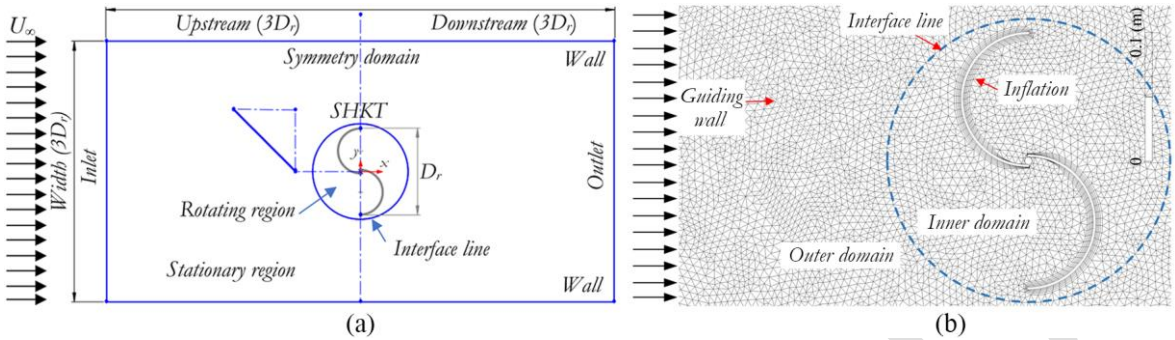

Figure 4. (a) A symmetry computational domain for two-dimensional CFD analyses and **(b)** Mesh configurations.

2.2.3. Turbulence models and mesh configurations

For a realistic simulation of flow across a SHKT model, several turbulence models have been considered. Typically, the Reynold-Averaged Navier-Stokes (RANS) method is the fastest CFD approach and widely utilised to solve the complex flow problems as a SHKT model. There is no agreement on the most appropriate model adopted in CFD simulations even in the two or three dimensions. To solve two separated transport equations which are the turbulent kinetic energy (k) equation and dissipation rate (ε) of turbulent kinetic energy equation, the simplest turbulence model widely accepted is the standard k-ε model (Sarma *et al*., 2014; Roy & Saha, 2013a; Roy & Saha, 2013b). Besides that, this model is suitable for flow with fully turbulent (Talukdar *et al*., 2018). In term of accuracy, the standard k-ε model showed a general agreement with experimental data, or was compared with other models in the published computational results (M. A. Kamoji *et al*., 2009, Roy and Saha 2013a, Kumar and Saini 2017, Saad *et al*., 2020). Therefore, the standard k-ε model together with a scalable wall function was employed in the present studies.

An ANSYS Fluent solver was used. The dynamic mesh motion technique suited for the boundary movement and together with three dynamic mesh methods; Smoothing, Layering and Remeshing was applied. Figure 4(b) illustrates the details of mesh configurations. The unstructured triangular meshes in the outer and inner domains were applied using the ANSYS meshing tool. A mesh independence study was conducted and found that the level six of mesh refinement with maximum of 0.005 m element size was good enough to use and was imposed. Moreover, the boundary layers were set using the inflation rate with a smooth transition and 1.2 of growth rate on the turbine bucket surfaces.

3. Results and Discussions

3.1. Effects of the Central Shaft

The effects of a central shaft were carried out by using 2D ANSYS Fluent simulations. The performances of a SHKT theoretically can be considered by generated torque and power. The starting torque ability represented in terms of the instantaneous torques in one revolution (0^o to 360^o) with the variation of constant upstream velocity (U_∞) including 0.3, 0.5, 0.8 and 1.1 m/s is shown in Figure 5. It can be observed that a SHKT without a central shaft provided the lowest torque compared to the rest cases in every U_∞, and the instantaneous torques of the case (I) and (II) were similar. Besides that, when U_∞ increases, the amplitude of instantaneous torques also increases.

The variation of maximum power output ($P_{m,\ max}$) as a function of the upstream velocity for all three cases is depicted in Figure 6(a). It shows that, when the upstream velocity was increased, $P_{m,\ max}$ was also increased. Additionally, $P_{m,\ max}$ of all cases was not significantly different when U_∞ was equal or lower than 0.5 m/s. However, $P_{m,\ max}$ of case II was slightly higher than the rest of cases when U_∞ was equal or higher than 0.8 m/s. The torque coefficient from the present study was compared with torque (Yaakob *et al*., 2010), and torque coefficient (Menet *et al*., 2004, M. A. Kamoji *et al*., 2009, M. A. Kamoji *et al*., 2009, Saad *et al*., 2020) of the previous studies from literatures as shown in

Figure 6 (b).

Figure 7 shows the velocity and pressure contours across a SHKT model from all three cases at fixed U_∞ = 0.8 m/s and $\theta = 45^o$. The results of every U_∞ provided similar characteristics of velocity and pressure contours. However, based on the results as shown in Figure 6(a), a little bit difference of $P_{m,\ max}$ from each case can be observed clearly when U_∞ was 0.8 m/s. Hence, U_∞ of 0.8 m/s was chosen to present the flow behaviours across a SHKT model. Based on the CFD results of case III shown in Figure 7, it can be observed that water is able to flow passing through the gap between turbine buckets contributed to the decreasing of pressure indicated from the colour contour inside a concave surface, and pressure difference between the convex and concave surfaces of a bucket. In fact, the pressure difference plays an important role on a generated torque. Therefore, the generated torque from this case is lower than case I and case II. In addition, the results from case I and case II were not much different from each other, although there was a small gap in case II. However, that gap was too small compared to the diameter of a central shaft. In addition, some flow structures can be noticed. These were the recirculation flow regions on the convex sides, and counter rotating vortices. These flow structures depicted in Figure 7 directly affect SHKT performances.

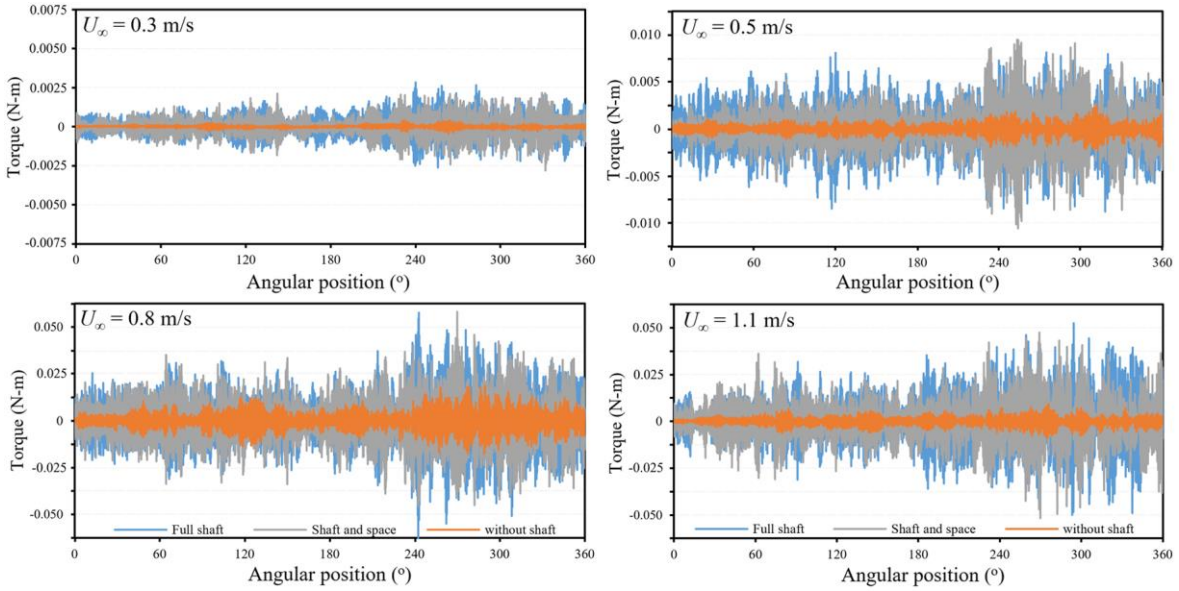

Figure 5. The variation of instantaneous torque from the effects of a central shaft for all 3 cases at U_∞ = 0.3, 0.5, 0.8, and 1.1 m/s.

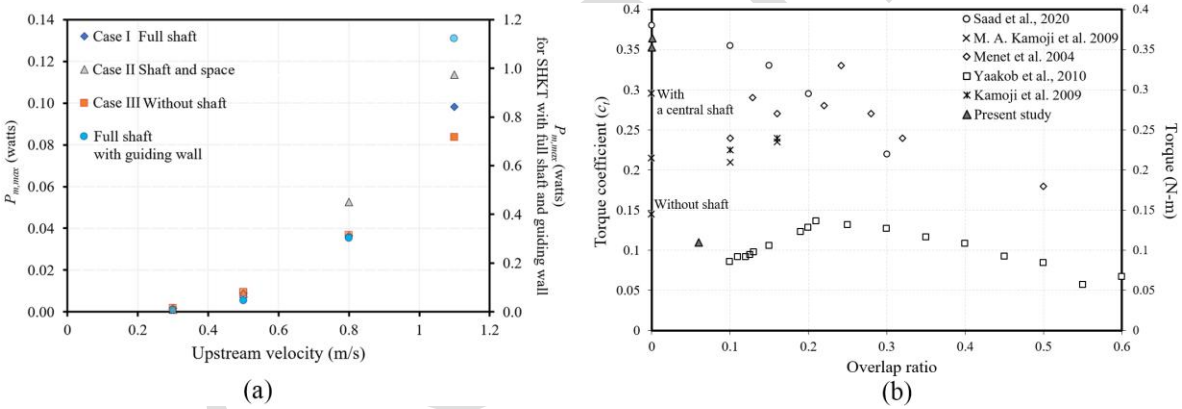

Figure 6. (a) Variation of maximum power output; $P_{m,max}$ (watts) with upstream velocity; U_∞ (m/s), and **(b)** comparison the results from present studies with previous studies.

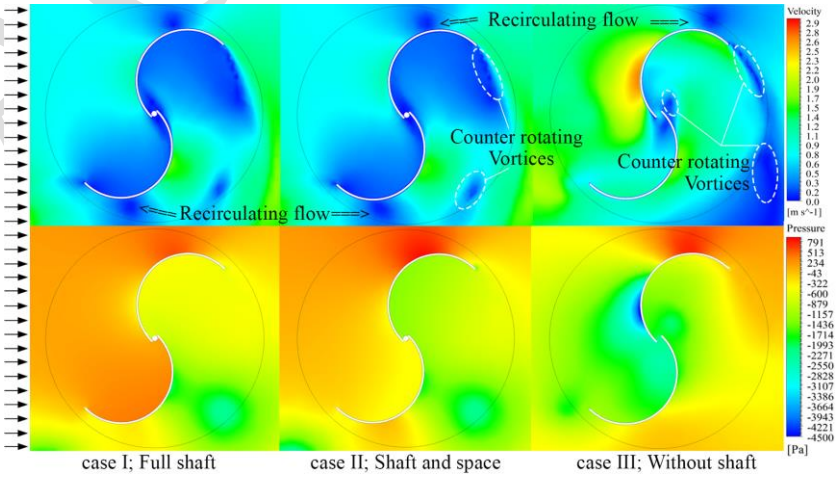

Figure 7. Pressure and velocity contours across SHKT models of all three cases at fixed U_∞ = 0.8 m/s and θ = 45°.

3.2. Effects of a Guiding Wall

A full shaft SHKT model (case I) from the previous section was selected because it provided the optimum overall performances, and was modified by adding a guiding wall. The simulations were carried out by using one upstream velocity (U_∞) of 0.5 m/s. As mentioned in the previous section, the power coefficient is increased when U_∞ is increased. Thus, U_∞ of 0.5 m/s was selected to investigate the influence of a guiding wall on a full shaft SHKT model whether it can increase the power coefficient becoming equalled or higher when U_∞ = 0.8 or 1.1 m/s. $P_{m,\,max}$ of a full shaft SHKT model with a guiding wall was compared with ones without a guiding wall. From the results shown in Figure 6(a), it can be seen that $P_{m,\,max}$ of a full shaft SHKT model with a guiding wall was the highest, and higher than $P_{m,\,max}$ of that one without a guiding wall about 10–13 times.

The variation of c_p and instantaneous torque with angular positions (θ) for a full shaft SHKT model with and without a guiding wall at fixed U_∞ = 0.5 m/s are illustrated in Figure 8. As seen in the figure, a full-shaft SHKT model with a guiding wall shows less fluctuation of torque and a greater peak of c_p than that one without a guiding wall.

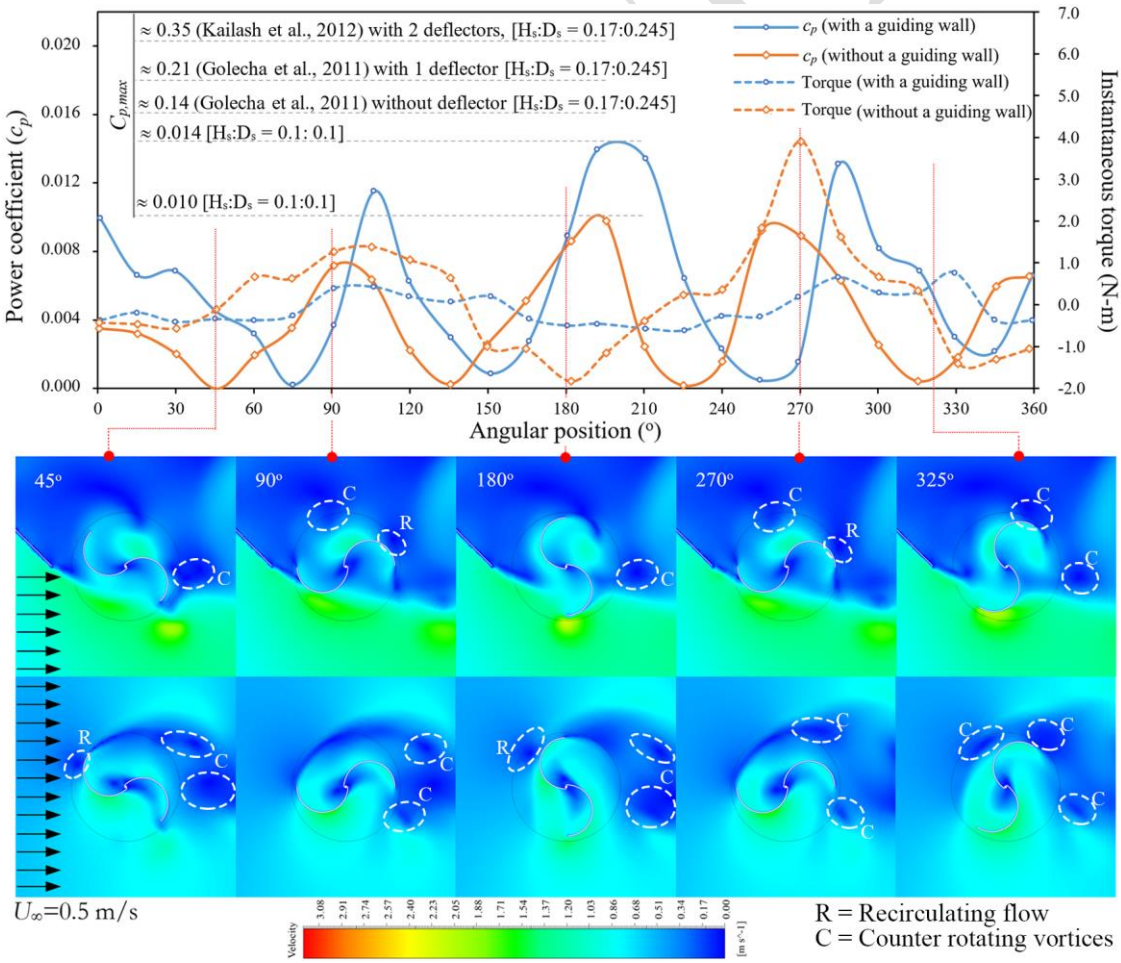

Figure 8. The variation of c_p and instantaneous torque with angular positions, and the velocity contours of a full-shaft SHKT model with and without a guiding wall at fixed U_∞ = 0.5 m/s.

Furthermore, the c_p of the full shaft SHKT model with and without a guiding wall started to increase when θ is about 75º, 150º, 260º, and 340º and 45º, 135º, 225º and 315º, respectively. Having a 45º guiding wall changes the water direction and c_p, hence is shifted around 25º–30º behind the other one. It is noticed that the c_p increasing ranges of angles occurred when bucket A was forced and accelerated from water flowing through it. Whereas, the decreasing range occurred when SHKT buckets lost their momentum due to the decreasing of hydrodynamic force, leading to the decreasing of rotational speed and corresponding with the decreasing of c_p at that range of angular positions. In addition, velocity contours in Figure 8 show flow field across a full-shaft SHKT model without and with a 45º guiding wall with U_∞ of 0.5 m/s at θ = 45º, 90º, 180º, 270º and 325º. Flow structures which are counter rotating vortices and recirculating flow areas can be observed from both cases. When θ = 45º, 180º and 325º, c_p of a full-shaft SHKT model with a guiding wall was higher because of smaller counter rotating vortices, and no have recirculating flow at a concave surface of a returning bucket. On the other hand, c_p of that case was lower when θ = 90º, and 270º, due to the occurrence of recirculating flow and counter rotating vortices.

Other than the flow field characteristics across a SHKT model, pressure distribution and the pressure difference between the convex and concave sides of buckets also affect the performances as shown in Figure 9. This is consistent with the c_p plot shown in Figure 8.

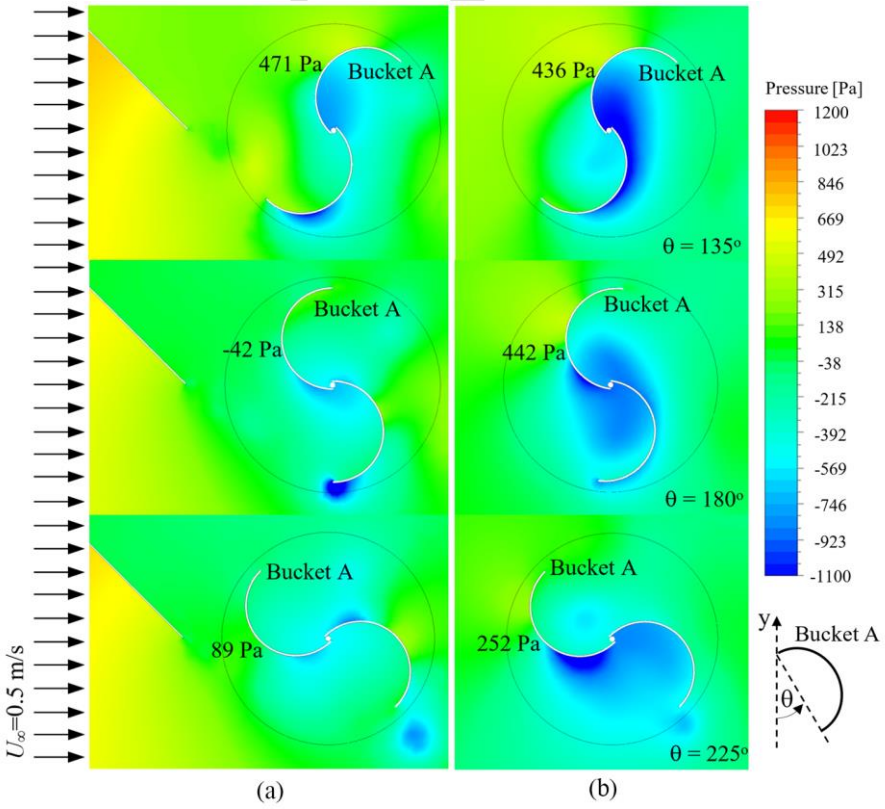

Figure 9. The pressure contours of a full-shaft SHKT buckets in case of **(a)** with a guiding wall and **(b)** without a guiding wall at bucket positions θ = 135º, 180º and 225º for fixed U_∞ = 0.5 m/s.

When bucket A changes from being an advancing bucket into a returning bucket (θ = 180^o), bucket A is suffering from drag force or high pressure from the incoming fluid flow and hence generates the opposite torque direction. At that angular position, the pressure on a convex surface of bucket A is equal -42 Pa and 442 Pa for a SHKT model with and without a guiding wall, respectively. Thus, c_p with a guiding wall increases surpassing the one without. Furthermore, pressure along the concave surface is also important. When θ = 135^o, the pressure inside a bucket A of a full-shaft SHKT model with a guiding wall is greater than a model without a guiding wall, leading to high c_p even though the pressure on the convex surface is high. When θ = 225^o, a SHKT model with a guiding wall has a lower pressure on the convex surface and higher pressure on the concave surface of a bucket A contributing to higher c_p. However, that is a declining state because the momentum of a SHKT model was decreasing. Hence the c_p was also decreasing.

Finally, the comparison between the performances of a SHKT model with a guiding wall in this study and in previous studies also proved and emphasised the necessity of the presence of a guiding wall that not only augments turbine performances where $c_{p,\ max}$ increases 40% compared to the one without a guiding wall, but it also enhances the hydrodynamics behaviour of water flowing through a SHKT model as well. This is consistent with the results from the experimental study by Golecha *et al*. (2011) and Kailash *et al*. (2012) as indicated in Figure 8. It was seen that, the $c_{p,\ max}$ from studies of those authors was higher. However, the turbine size or an aspect ratio (H_s/D_r) also affects directly on turbine performances (Mahmoud *et al*., 2012, Zhao *et al*., 2009, M. A. Kamoji *et al*., 2009, M. A. Kamoji *et al*., 2009). Therefore, the fair comparison needs to be carried out by the $c_{p,\ max}$ per projected area ($H_s \times D_r$) of the turbine where H_s is turbine height and D_r is rotor diameter. Based on the CFD results in this study, it can be proved that a full shaft SHKT model with a guiding wall provides better $c_{p,\ max}$ per projected area than previous study.

4. Conclusions

The 2D computational methodology using ANSYS Fluent with a k-ε turbulence model was utilised to investigate the effects of a central shaft design and a guiding wall on the SHKT performances including generated torque and power coefficient. The major conclusions can be summarised as follows:

- The spaces between turbine buckets play vital roles on hydrodynamic behaviour around the turbine central shaft and affect mainly to the drag force along both sides of SHKT buckets leading to the variation on turbine torque. CFD simulation results on the effects of the central shaft design show that a SHKT model with a full shaft (case I), (β = 0) gives the starting torque capability similar to case II, (β = 0.0009). Both of these designs are more efficient compared to case III, a SHKT model without shaft between end plates in terms of torque performance or starting torque, and maximum power output.

- Finally, a full-shaft SHKT with a guiding wall significantly provides more power coefficient and starting torque, and less torque fluctuation compared to without a guiding wall. There was an enhancement in the maximum power by 10–13 times, and maximum power coefficient around 40% compared to a full shaft SHKT without a guiding wall. The benefits of a guiding wall are not only to protect the returning bucket from floating debris, rubbles or settlings, but it is also able to reduce drag force on the returning bucket leading to a significant increase of the power coefficient.

Author Contributions: Conceptualisation, K. Tantichukiad.; writing—review and editing, K. Tantichukiad, A. Yahya, A.S. Mohd Rafie, A. Mohd Mustafah, H. H. Harith and A. S. Mat Su.; methodology and simulation, K. Tantichukiad.; writing—original draft preparation, K. Tantichukiad.; writing—review and editing, K. Tantichukiad, A. Yahya, A.S. Mohd Rafie, A. Mohd Mustafah, H. Haizi Harith and A. S. Mat Su.

Funding: This work was funded by SEARCA.

Conflicts of Interest: The authors declare no conflict of interest.

References

Akwa, Vicente, J., Gilmar Alves d. S. J., *et al*. (2012). Discussion on the verification of the overlap ratio influence on performance coefficients of a Savonius wind rotor using computational fluid dynamics. *Renewable Energy*, *38*(1), 141–49.

Akwa, Vicente, J., Vielmo, H. A. *et al*. (2012). A review on the performance of Savonius wind turbines. *Renewable and Sustainable Energy Reviews*. *16*(5). 3054–64.

Altan, B. D. & Atilgan, M. (2008). An experimental and numerical study on the improvement of the performance of Savonius wind rotor. *Energy Conversion and Management*. *49*(12), 3425–32.

Damak, A., Driss, Z., & Abid, M. S. (2013). Experimental investigation of helical Savonius rotor with a twist of 180°. *Renewable Energy*. *52*, 136–42.

El-Askary, W. A., Nasef, M. H., AbdEL-hamid, A. A., *et al*. (2015). Harvesting wind energy for improving performance of Savonius rotor. *Journal of Wind Engineering and Industrial Aerodynamics*. *139*, 8–15.

Fujisawa, N. (1992). On the torque mechanism of Savonius rotors. *Journal of Wind Engineering and Industrial Aerodynamics*. *40*(3), 277–92.

Golecha, Kailash, Eldho, T. I., *et al*. (2011). Influence of the deflector plate on the performance of modified Savonius water turbine. *Applied Energy*. *88*(9), 3207–17.

Jahangir Alam, M., & Iqbal, M. T., (2009). "Design and development of hybrid vertical axis Turbine." Pp. 1178–83 in *Canadian Conference on Electrical and Computer Engineering*.

Jeon, Keum Soo, Jun, I. J.., Jae, K. P., *et al*. (2015). Effects of end plates with various shapes and sizes on helical Savonius wind turbines. *Renewable Energy*. *79*(1): 167–176.

Kacprzak, Konrad, Grzegorz L., *et al*. (2013). Numerical investigation of conventional and modified Savonius wind turbines. *Renewable Energy*. *60*, 578–85.

Kailash, Golecha, Eldho, T. I., *et al*. (2012). Performance study of modified savonius water turbine with two deflector plates. *International Journal of Rotating Machinery* 2012.

Kamoji, M. A., Kedare, S. B., & Prabhu, S. V. (2009). Experimental investigations on single stage modified Savonius rotor. *Applied Energy*. *86*(7–8), 1064–73.

Kamoji, M. A., Kedare, S. B., & Prabhu, S. V., (2009). Performance tests on helical Savonius rotors. *Renewable Energy*. *34*(3): 521–29.

Kerikous, Emeel, & Dominique T., (2019). Optimal shape and position of a thick deflector plate in front of a hydraulic Savonius turbine. *Energy*. *189*: 116157.

Kianifar, A. & Anbarsooz, M., (2011). Blade curve influences on the performance of Savonius rotors: experimental and numerical. *Proceedings of the Institution of Mechanical Engineers, Part A: Journal of Power and Energy*. *225*(3), 343–350.

Kumar, Anuj & Saini, R. P., (2016). Performance parameters of Savonius type hydrokinetic turbine – A review. *Renewable and Sustainable Energy Reviews*. *64*, 289–310.

Kumar, Anuj & Saini, R. P., (2017). Performance analysis of a single stage modified Savonius hydrokinetic turbine having twisted blades. *Renewable Energy*. *113*, 461–78.

Mabrouki, Ibrahim, Driss, Z., *et al*. (2014). Performance analysis of a water Savonius rotor: effect of the internal overlap. *Sustainable Energy*. *2*(4): 121–125.

Mahmoud, N. H., El-Haroun, A. A., Wahba, E., *et al*. (2012). An experimental study on improvement of Savonius rotor performance. *Alexandria Engineering Journal*. *51*(1): 19–25.

Mendoza, Victor, Katsidoniotaki, E., *et al*. (2020). Numerical study of a novel concept for manufacturing Savonius turbines with twisted blades. *Energies*, *13*(8).

Menet, Jl, J. L., Bourabaa, N., *et al*.. (2004). Increase in the Savonius rotors efficiency via a parametric investigation. *EWEA - 2004 European Wind Energy Conference* (April).

Mohamed, M. H., Janiga, G., Pap, E., *et al*. (2010). Optimisation of Savonius turbines using an obstacle shielding the returning blade. *Renewable Energy*, *35*(11): 2618–2626.

Roy, Sukanta & Ujjwal K. Saha. (2013a). Computational study to assess the influence of overlap ratio on static torque characteristics of a vertical axis wind turbine. *Procedia Engineering*, *51*, 694–702.

Roy, Sukanta & Ujjwal K. Saha. (2013b). Review on the numerical investigations into the design and development of Savonius wind rotors. *Renewable and Sustainable Energy Reviews*. *24*, 73–83.

Saad, Ahmed, S., Ibrahim, I. El-Sharkawy, Ookawara, S., *et al*. (2020). Performance enhancement of twisted-bladed Savonius vertical axis wind turbines. *Energy Conversion and Management*. 209, 112673.

Sarma, N. K., Biswas, A., & Misra, R. D., (2014). Experimental and computational evaluation of Savonius hydrokinetic turbine for low velocity condition with comparison to Savonius wind turbine at the same input power. *Energy Conversion and Management*, *83*, 88–98.

Sivasegaram, S., (1978). Secondary parameters affecting the performance of resistance-type vertical-asix wind rotors. *Wind Engineering*, *2*(1), 49–58.

Talukdar, Parag, K., Sardar, A., *et al*. (2018). Parametric analysis of model Savonius hydrokinetic turbines through experimental and computational investigations. *Energy Conversion and Management*, *158*, 36–49.

Yaakob, O., Tawi, K. B., *et al*. (2010). Computer simulation studies on the effect overlap ratio for Savonius type vertical axis marine current turbine. *International Journal of Engineering*, *23*(1), 79–88.

Zhao, Zhenzhou, Yuan Zheng, *et al*. (2009). Research on the improvement of the performance of Savonius rotor based on numerical study. in *1st International Conference on Sustainable Power Generation and Supply, SUPERGEN '09*.